



On the mathematical model of Eyring–Powell nanofluid flow with non-linear radiation, variable thermal conductivity and viscosity

Matthew O. Lawal^a, Kazeem B. Kasali^b, Hammed A. Ogunseye^c, Michael O. Oni^d,
Yusuf O. Tijani^{e,*}, Yussuff T. Lawal^f

^a Department of Mathematics, Adeyemi College of Education, Ondo, Nigeria

^b Department of Mathematics and Statistics, First Technical University, Ibadan, Nigeria

^c School of Mathematics, Statistics and Computer Science, University of KwaZulu-Natal – Pietermaritzburg Campus, Pietermaritzburg, South Africa

^d Department of Mathematics, Ahmadu Bello University, Zaria, Nigeria

^e Department of Mathematics and Applied Mathematics, Nelson Mandela University, Port Elizabeth, South Africa

^f Department of Mathematics, Obafemi Awolowo University, Ile-Ife, Nigeria

ARTICLE INFO

Keywords:

Nanofluid
Eyring–Powell
Stretching sheet
Brownian motion
Thermophoresis effect

ABSTRACT

It is well known that the significance of dynamic viscosity and thermal conductivity cannot be overemphasized in the movement of any fluid. In the present investigation, the impact of variable viscosity, variable thermal conductivity, Brownian motion, thermophoresis, heat and chemical reaction effects on an unsteady Eyring–Powell nanofluid flow in a stretching sheet is extensively discussed. The governing non-linear coupled partial differential equations describing the problem were derived. Similarity variables were used to transform the governing partial differential equations into ordinary differential equations. After which the Spectral quasi-linearization method (SQLM) was employed to numerically handle the emerging governing differential equations after validating the convergence of the method with existing results in literature. The novel flow features which include fluid velocity, skin friction, heat transfer coefficient and rate of mass transfer were discussed therein as a function of sundry parameters entering flow formation. Findings reveal that the Brownian motion and thermophoresis parameters increase the temperature profile. Also, fluid concentration was found to be a decreasing and increasing function of Brownian motion parameter and thermophoresis parameter respectively. For accuracy check, tabular representations are carried out with published work in the literature; excellent agreement were found.

1. Introduction

The word *nanofluid* describes a liquid coolant formed by the presence of one or more sub-micronic solid particles (nanoparticles), primarily used as heat transfer equipment such as radiators, electronic cooling system (such as flat plates) and heat exchangers. Many articles deal with understanding the behaviour of nanofluids to determine appropriate choice to enhance heat transfer in industrial applications such as; microelectronics, fuel cells, nuclear reactors, transportation, hybrid-powered, domestic refrigerator engine as well as biomedicine and food storage. This term was first used by Choi¹ where he discussed how nanofluids can be used to enhance thermal conductivity. Similar results have been established by various researchers over the years, to mention a few; Masuda et al.² examined the alteration of thermal conductivity and viscosity of liquid. Buongiorno³ gave a mathematical model that incorporated the thermophoresis and Brownian motion effects, Khanafer et al.⁴ and Abu-Nada.⁵ Other related articles where the mathematical

model of Buongiorno³ is employed include (Neild and Kuznetsov⁶ and Grosan and Pop⁷). Flow formations due to stretching sheet has significant industrial applications such as plastic fabrications, the hot rolling wire drawing and glass–fibre production. Based on these applications, one of the earliest work on flow formation due to stretching sheet is the work of Sarkiadis⁸ where the forced convection boundary layer flow past a moving flat plate was studied. After which several authors have conducted different physical situations of the aforementioned problem. Cran⁹ studied the steady laminar boundary layer flow of a Newtonian fluid caused by a stretching plate while Magyari and Keller¹⁰ offered exact solutions for the problem, Ishak et al.¹¹ studied the same problem over an unsteady stretching vertical surface, while Wang¹² discovered an unusual type of flow due to shrinking when the behaviour of a liquid film on an unsteady stretching sheet was investigated. Kasali et al.¹³ probed the significance of Soret and Dufour on the flow of a second grade fluid over a surface stretched exponentially using a modified (Cattaneo–Christov) heat flux model. The homotopy analysis

* Corresponding author.

E-mail address: olodyusuf@gmail.com (Y.O. Tijani).

method was employed to solve the governing flow equations. Their study elucidated that increase in Dufour parameter support the fluid thermal boundary layer while an opposing trend was noticed for Soret parameter.

The classical Newtonian fluids have several limitations in giving accurate prediction of flow formations and heat transfer whenever the shear stress and strain are not linear. Meanwhile, in application, most industrial fluids are non-Newtonian; such as paint, blood, crude-oil, ketchups and starch. For proper understanding and physical analysis of this kind of fluids (non-Newtonian fluids), several models over the years have been proposed; such as the power law model, the Casson fluid model, Maxwell fluid, Jeffrey fluid, Eyring–Powell fluid. For this current investigation, we have employed the Eyring–Powell fluid model proposed by Eyring and Powell.¹⁴ One distinctive feature of the Eyring–Powell fluid is that it has its understanding from the molecular theory and not from empirical relation which most Non-Newtonian fluids are derived from. Several research articles have been committed to comprehend this type of fluid. By the use of Keller box method, Javed et al.¹⁵ considered the Eyring–Powell fluid flow model over a stretching sheet. They concluded that there exists enhanced velocity profiles for a non-Newtonian fluid, as against the use of a Newtonian fluid. On the other hand Hayat et al.¹⁶ gave series solution for heat transfer in an Eyring–Powell fluid flow over a continuously moving surface with a convective boundary condition by means of the homotopy analysis method. Recently, Ogunseye et al.¹⁷ scrutinized the stagnation-point of Eyring–Powell nanofluid over stretching cylinder with thermal slip jump by incorporating the buoyant force. They concluded that the skin friction is enhanced by the velocity slip parameter and the fluid material parameter. In another work, the entropy generation due to irreversibility ratio in an unsteady Eyring–Powell hybrid nanofluid over a permeable surface was carried out by Ogunseye et al.¹⁸ using a Lie-group analysis. They established through analysis that entropy generation is minimize in the system by a decrease in Eckert number and nanoparticle volume fraction. Also, Ogunseye et al.¹⁹ examined the dynamical behaviour of Eyring–Powell nanofluid through parallel horizontal plate with heat-dependent thermal conductivity, chemical reaction and magnetic field under the influence of thermophoresis and Brownian motion. They established that hydromagnetic Brownian parameter and thermophoresis parameter influence greatly the heat and mass transfer as shown by the flow profiles. Other related works where the Eyring–Powell nanofluid flow is discussed are; Akbaret al.²⁰, Agbaje et al.²¹ and Ibrahim and Gadisa²² where they found numerical solution for Powell–Eyring nanofluid in the presence of transversely applied magnetic field, heat generation and non-linear stretching surface respectively, Babu et al.²³ discussed the heat and mass transfer in MHD Eyring–Powell nanofluid flow due to cone in porous medium, Jalil et al.,²⁴ Hayat et al.,²⁵ Ramzan et al.²⁶ and Malik et al.²⁷ The significance of heat source in moving fluids is of great importance in view of its numerous physical applications such as those dealing with chemical reactions and those concerned with dissociating fluids.

Over the years, several models have been mathematically rendered for the understanding of internal heat generation effect on flow formations; Inman²⁸ and Ostrach²⁹ assumed it to be constant while it is considered as a function of space by Toor³⁰ and Chambre.³¹ Later, Foraboschi and Federico,³² presented the volumetric rate of heat generation to be directly proportional to $(T - T_0)$ and disclosed that it is an approximation of the state of some exothermic process with T_0 as the initial temperature. In other work, Jha and Ajibade³³ probed the transient natural convection flow of heat generating/absorbing fluid between vertical porous plates with periodic heat input. They established that, the effect of heat sink is inhibited by large suction value and the impact of suction/injection is suppressed by large value of heat sink. Later, Adesanya,³⁴ studied the free convective flow of heat generating fluid through a porous vertical channel with slip velocity and jump temperature. He established that increase in slip and temperature jump parameters increases the periodic flow velocity and fluid

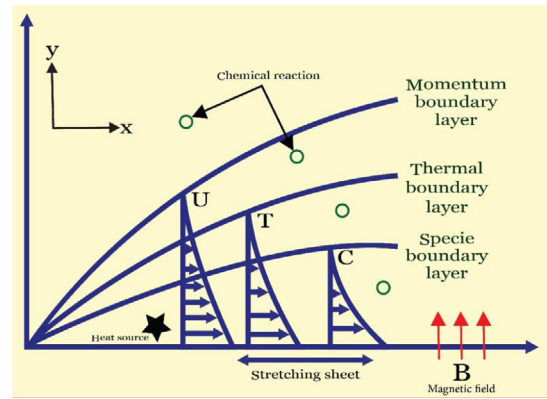


Fig. 1. Flow geometry.

temperature respectively. Jha et al.³⁵ scrutinized steady fully developed mixed convection flow in a vertical micro-concentric-annulus with heat generating/absorbing fluid and reported that increase in heat generation/absorption parameter decreases rate of heat transfer at the outer surface of inner cylinder. While Oni³⁶ analytically discussed the role of heat source on mixed convection flow in a vertical annulus filled with porous materials in the presence of thermal radiation. Despite all of the above contributions, no research work has been done to derive a mathematical model for Eyring–Powell nanofluids with Brownian and thermophoresis effects in the presence of a heat source and a chemical reaction, taking variable viscosity and thermal conductivity into account, to the best of the authors' knowledge. The purpose of this paper is to determine the impact of various parameters entering flow formation on heat and mass transfer. The current study has immense industrial and technological applications such as in metal extrusion, solar heating, electronic devices, polymeric sheets, energy production, food processing and other manufacturing processes.

2. Organization of the paper

The paper is set up as follows. The governing mathematical equations describing the aforementioned problem are presented in Section 3, while the numerical procedure in solving the coupled nonlinear partial differential equations using the spectral quasi-linearization method (SQLM) lies in Section 4. Section 5 is devoted to discussion of results, based on numerical values obtained and depicted graphs, while the salient conclusions are drawn in Section 6.

3. Model formulation analysis

We consider a 2-dimensional flow of an unsteady incompressible chemically reactive Eyring–Powell nanofluid over a stretching surface. The stretching sheet velocity is assumed to vary in a linear manner. The viscosity and thermal conductivity are linearly dependent on temperature. The magnetic field acting normal to the flow direction is assumed to be constant. Nonlinear thermal radiative heat flux in the full form is employed without the usual truncation of the higher order terms in the expansion with the effect of Brownian motion, heat source and thermophoresis considered in the flow analysis. The influence of ion-slip, thermoelectric, Hall current and Joule heating (Ohmic dissipation) are ignored as well as buoyancy forces, see Ogunseye et al.¹⁸ and Mkhathswa et al.³⁷ Thus, some of the assumptions governing the study are stated (see Fig. 1).

$$\frac{\partial u}{\partial x} + \frac{\partial v}{\partial y} = 0, \quad (3.1)$$

$$\frac{\partial u}{\partial t} + u \frac{\partial u}{\partial x} + v \frac{\partial u}{\partial y} = \frac{1}{\rho} \frac{\partial}{\partial y} \left(\mu(T) \frac{\partial u}{\partial y} \right) + \frac{1}{\rho \beta \gamma} \frac{\partial^2 u}{\partial y^2} - \frac{1}{2\rho \beta \gamma^3} \left(\frac{\partial u}{\partial y} \right)^2 \frac{\partial^2 u}{\partial y^2} - \frac{\sigma B_0^2 u}{\rho}, \quad (3.2)$$

$$\begin{aligned} \frac{\partial T}{\partial t} + u \frac{\partial T}{\partial x} + v \frac{\partial T}{\partial y} &= \frac{1}{(\rho c_p)} \frac{\partial}{\partial y} \left(k(T) \frac{\partial T}{\partial y} \right) - \frac{1}{(\rho c_p)} \frac{\partial q_r}{\partial y} \\ &+ \tau \left[D_B \frac{\partial C}{\partial y} \frac{\partial T}{\partial y} + \frac{D_T}{T_\infty} \left(\frac{\partial T}{\partial y} \right)^2 \right] + \frac{q''' }{\rho c_p} \\ &+ \frac{1}{(\rho c_p)} \left[\left(\mu(T) + \frac{1}{\beta \gamma} \right) \left(\frac{\partial u}{\partial y} \right)^2 - \frac{1}{6\beta \gamma^3} \left(\frac{\partial u}{\partial y} \right)^4 \right] + \frac{\sigma B_0^2 u^2}{\rho c_p}, \end{aligned} \tag{3.3}$$

$$\frac{\partial C}{\partial t} + u \frac{\partial C}{\partial x} + v \frac{\partial C}{\partial y} = D_B \frac{\partial^2 C}{\partial y^2} + \left(\frac{D_T}{T_\infty} \right) \frac{\partial^2 T}{\partial y^2} - k(t)(C - C_\infty), \tag{3.4}$$

where

$$\begin{cases} q''' = \frac{k_* u_w}{x v_f} \left[H(T_w - T_\infty) f' + H^*(T - T_\infty) \right], \\ \mu(T) = \mu_\infty [1 - \xi(T - T_\infty)], \quad k(T) = k_\infty [1 + \chi(T - T_\infty)], \\ q_r = -\frac{4\sigma' \partial T^4}{3k \partial y}. \end{cases} \tag{3.5}$$

The associated boundary conditions are given as;

$$u = u_w(x) = \frac{cx}{1 - \lambda t}, \quad v = v_w, \quad T = T_w, \quad C = C_w \quad \text{at} \quad y = 0. \tag{3.6}$$

$$u \rightarrow 0, \quad T \rightarrow T_\infty, \quad C \rightarrow C_\infty \quad \text{at} \quad y \rightarrow \infty. \tag{3.7}$$

Where $\tau = \frac{(\rho c_p)_p}{(\rho c_p)_f}$ depicts the ratio of the heat capacitant of the nanoparticle material and heat capacitant of the fluid, u and v are the velocity components in x and y axes respectively. T and C represent the temperature and concentration of the fluid respectively. β and γ are the fluid parameters (Eyring–Powell). ρ is the fluid density, $\mu(T)$ and $K(T)$ are temperature dependent dynamical viscosity and thermal conductivity. μ_∞ and k_∞ are viscosity and thermal conductivity of the fluid far away from the stretching sheet, ξ is the variable dynamical viscosity parameter that quantifies the rate at which viscosity changes with temperature. χ is the variable thermal conductivity parameter that quantifies the rate at which thermal conductivity changes with temperature. B_0 is the intensity of magnetic field, D_B and D_T are Brownian motion diffusion and thermophoretic diffusion coefficient in that order. q_r and q''' stands for radiation and heat source effect respectively. k is the mean absorption coefficient, σ' is the Stefan-Boltzmann constant, c is the stretching parameter. Where $k(t) = \frac{k'_r}{(1-\lambda t)}$ is the chemical reaction coefficient, H and H^* are the coefficient of space and temperature dependent heat source/sink. We consider the wall temperature T_w and nanoparticle concentration C_w as

$$T_w(x, t) = T_\infty + \frac{ax}{1 - \lambda t}, \quad C_w(x, t) = C_\infty + \frac{bx}{1 - \lambda t},$$

a and b are positive constants and λ is a positive constant having dimension $time^{-1}$.

By employing the similarity variables

$$\begin{cases} \eta = \sqrt{\frac{c}{v(1-\lambda t)}} y, \quad \psi = \sqrt{\frac{cv}{(1-\lambda t)}} x f(\eta), \quad u = \frac{cx}{1-\lambda t} f'(\eta), \\ v = -\sqrt{\frac{cv}{(1-\lambda t)}} f(\eta), \quad \theta(\eta) = \frac{T - T_\infty}{T_w - T_\infty}, \\ \phi(\eta) = \frac{C - C_\infty}{C_w - C_\infty}. \end{cases} \tag{3.8}$$

Eqs. (3.1)–(3.7) become

$$\begin{aligned} (1 + \epsilon - \beta_1 \theta) f'''' - \beta_1 \theta' f''' + f f'' - (f')^2 - \epsilon \delta (f'')^2 f''' \\ - \Lambda \left(f' + \frac{\eta}{2} f'' \right) - M f' = 0. \end{aligned} \tag{3.9}$$

$$\begin{aligned} (1 + \beta_2 \theta) \theta'' + \beta_2 (\theta')^2 \\ + \frac{4}{3} R \left[3(1 + (\theta_w - 1)\theta)^2 (\theta_w - 1)\theta'^2 + (1 + (\theta_w - 1)\theta)^3 \theta'' \right] + Pr \lambda_1 f' \\ + Pr \lambda_2 \theta + Pr Ec \left((1 - \beta_1 \theta + \epsilon) f''^2 - \frac{\epsilon \delta}{3} (f'')^4 \right) + Pr Ec M f'^2 \\ - Pr \Lambda \left(\theta + \frac{\eta}{2} \theta' \right) \\ + Pr Nb \phi' \theta' + Pr Nt \theta'^2 + Pr f \theta' - Pr f' \theta = 0. \end{aligned} \tag{3.10}$$

$$\phi'' + \frac{Nt}{Nb} \theta'' + Pr Le \left[f \phi' - f' \phi - \Lambda \left(\phi + \frac{\eta}{2} \phi' \right) - k_r \phi \right] = 0. \tag{3.11}$$

We observed the satisfaction of the continuity equation in Eq. (3.1). In addition, the appropriate boundary conditions in dimensionless form are transformed to:

$$f(0) = 0, \quad f'(0) = 1, \quad f'(\infty) \rightarrow 0, \tag{3.12}$$

$$\theta(0) = 1, \quad \theta(\infty) \rightarrow 0, \tag{3.13}$$

$$\phi(0) = 1, \quad \phi(\infty) \rightarrow 0. \tag{3.14}$$

with the following relevant dimensionless parameter

$$\begin{cases} \Lambda = \frac{\lambda}{c}, \quad \beta_1 = \xi(T_w - T_\infty), \quad \beta_2 = \chi(T_w - T_\infty), \\ \epsilon = \frac{1}{\beta \gamma \mu_\infty}, \quad \delta = \frac{cu_w^2}{2v\gamma^2(1-\lambda t)}, \quad K_r = \frac{k'_r}{c}, \quad M = \frac{\sigma B_0^2(1-\lambda t)}{c\rho}, \\ R = \frac{4\sigma' T_\infty^3}{k_1 \alpha}, \quad Nb = \frac{\tau D_B (C_w - C_\infty)}{v}, \quad Nt = \frac{\tau D_T (T_w - T_\infty)}{v T_\infty}, \quad \theta_w = \frac{T_w}{T_\infty}, \\ L_e = \frac{\alpha}{D_B}, \quad \lambda_1 = \frac{ak_*}{(\rho c_p)v}, \quad \lambda_2 = \frac{bk_*}{(\rho c_p)v}, \quad Pr = \frac{v}{\alpha}, \quad Ec = \frac{u_w^2}{c_p(T_w - T_\infty)}. \end{cases} \tag{3.15}$$

where M is the magnetic parameter, Pr stands for Prandtl number, Le is the Lewis number, Nb represents the Brownian parameter, Nt is the thermophoresis parameter, Ec is the Eckert number, K_r stands for the chemical reaction parameter, R represent the radiation parameter, λ_1 is the space generation/absorption parameter, λ_2 is the heat generation/absorption parameter, Λ is the unsteadiness parameter, θ_w represents temperature ratio, β_1 represents variable dynamical viscosity parameter, β_2 stands for variable thermal conductivity parameter. ϵ and δ are the Eyring–Powell fluid parameters.

The engineering physical parameter of skin friction coefficient, Nusselt and Sherwood numbers takes the following definition;

$$\begin{aligned} C_f &= \frac{\tau_w}{\rho u_w^2}, \\ Nu_x &= \frac{x q_w}{k_\infty (T_w - T_\infty)}, \\ Sh_x &= \frac{x q_m}{D_B (C_w - C_\infty)}. \end{aligned} \tag{3.16}$$

Where shear stress, surface heat flux and mass flux are τ_w , q_w and q_m which are defined as

$$\begin{aligned} \tau_w &= \left(\mu(T) + \frac{1}{\beta \gamma} \right) \left(\frac{\partial u}{\partial y} \right) - \frac{1}{6\beta \gamma^3} \left(\frac{\partial u}{\partial y} \right)^3 \Big|_{y=0}, \\ q_w &= -\left(k(T) + \frac{16\sigma' T^3}{3k} \right) \frac{\partial T}{\partial y} \Big|_{y=0}, \quad q_m = -D_B \frac{\partial C}{\partial y} \Big|_{y=0}. \end{aligned} \tag{3.17}$$

In dimensionless form, Eq. (3.16) using the definition of Eqs. (3.8), (3.15) and (3.17) becomes

$$\begin{aligned} Re_x^{\frac{1}{2}} C_f &= (1 - \beta_1 \theta(0) + \epsilon) f''(0) - \frac{\epsilon \delta}{3} f''^3(0), \\ Re_x^{-\frac{1}{2}} Nu &= -\left(1 + \beta_2 \theta(0) + \frac{4}{3} R \left((1 + (\theta_w - 1)\theta(0))^3 \right) \right) \theta'(0), \\ Re_x^{-\frac{1}{2}} Sh &= -\phi'(0). \end{aligned} \tag{3.18}$$

where $Re_x = \frac{x^2 c}{v(1-\lambda t)}$ is the Reynolds number.

4. Numerical procedures

The non-linear coupled ODEs in Eqs. (3.9)–(3.11) with its boundary conditions in Eqs. (3.12)–(3.14) are not amenable to compact solution, an approximate iterative numerical method would be sought. To this end, the spectral quasi-linearization method (SQLM) will be used in handling the coupled system equation. The SQLM is a product of two powerful methods; quasi-linearization (QLM) and spectral (Chebyshev) collocation (SCCM) methods. Quasi linearization method (QLM) is due to the work of Bellman and Kalaba³⁸ which is a generalization of the Newton–Raphson method and a detail explanation as to the use of SCCM can be found in the work of Motsa³⁹ and Motsa and Sibanda.⁴⁰ The choice of the SQLM is necessitated due to its accuracy in handling exponentially decaying solution profiles, see Akolade and Tijani.⁴¹

We linearize Eqs. (3.9)–(3.11) to have

$$\xi_{1,a} f_{a+1}''' + \xi_{2,a} f_{a+1}'' + \xi_{3,a} f_{a+1}' + \xi_{4,a} f_{a+1} + \xi_{5,a} \theta_{a+1}' + \xi_{6,a} \theta_{a+1} = R_{b_1} \quad (4.1)$$

$$\xi_{7,a} f_{a+1}'' + \xi_{8,a} f_{a+1}' + \xi_{9,a} f_{a+1} + \xi_{10,a} \theta_{a+1}' + \xi_{11,a} \theta_{a+1} + \xi_{12,a} \phi_{a+1}' + \xi_{13,a} \phi_{a+1} = R_{b_2} \quad (4.2)$$

$$\xi_{14,a} f_{a+1}' + \xi_{15,a} f_{a+1} + \xi_{16,a} \theta_{a+1}' + \xi_{17,a} \theta_{a+1} + \xi_{18,a} \phi_{a+1}' + \xi_{19,a} \phi_{a+1} = R_{b_3} \quad (4.3)$$

with it relevant boundary conditions as

$$f_{a+1}' = 1, f_{a+1} = 0, \theta_{a+1} = 1, \phi_{a+1} = 1 \quad \text{for } \eta = 0, \quad (4.4)$$

$$f_{a+1}' = 0, \theta_{a+1} = 0, \phi_{a+1} = 0 \quad \text{as } \eta \rightarrow \infty. \quad (4.5)$$

where the variable (coefficient) are given as

$$\left\{ \begin{array}{l} \xi_{1,a} = 1 + \varepsilon - \beta_1 \theta_a - \varepsilon \delta f_a''', \quad \xi_{2,a} = f_a - \beta_1 \theta_a' - 2\varepsilon f_a'' f_a''' - \frac{\Lambda \eta}{2}, \\ \xi_{3,a} = -2f_a' - \Lambda - M, \\ \xi_{4,a} = f_a'', \quad \xi_{5,a} = -\beta_1 f_a'', \quad \xi_{6,a} = \beta_1 f_a''', \\ \xi_{7,a} = 2P_r Ec(1 + \varepsilon - \beta_1 \theta_a) f_a''' - \frac{4}{3} Ec \varepsilon \delta f_a'''^3 \\ \xi_{8,a} = 2M Ec P_r f_a' + P_r \lambda_1 - P_r \theta_a, \quad \xi_{9,a} = P_r \theta_a', \\ \xi_{10,a} = \beta_2 \theta_a + 1 + \frac{4}{3} R(1 + (\theta_w - 1)\theta_a)^3 \\ \xi_{11,a} = 2\beta_2 \theta_a' + 8R(1 + (\theta_w - 1)\theta_a)^2 (\theta_w - 1)\theta_a' \\ \quad - \frac{1}{2} P_r \Lambda \eta + P_r N_b \phi_a' + 2P_r N_t \theta_a' + P_r f_a \\ \xi_{12,a} = \beta_2 \theta_a'' + \frac{4}{3} R \left(6(1 + (\theta_w - 1)\theta_a)(\theta_a - 1)^2 \theta_a'' \right. \\ \quad \left. + 3(1 + (\theta_w - 1)\theta_a) \theta_a'' (\theta_a - 1)^2 \right) + \\ P_r \lambda_2 - P_r \Lambda - P_r Ec \beta_1 f_a'' - P_r f_a' \\ \xi_{13,a} = P_r N_b \theta_a', \quad \xi_{14,a} = -P_r L_e \phi_a', \quad \xi_{15,a} = P_r L_e \phi_a', \\ \xi_{16,a} = \frac{Nt}{Nb}, \quad \xi_{17,a} = 1 \\ \xi_{18,a} = L_e P_r f_a - \frac{1}{2} P_r L_e \Lambda \eta, \quad \xi_{19,a} = -K_r L_e P_r - \Lambda L_e P_r - L_e P_r f_a' \end{array} \right. \quad (4.6)$$

After the QLM has been achieved for Eqs. (3.9)–(3.11), we set our focus on the spectral Chebyshev collocation method. We note that we now have a linear coupled differential system of equation with variable coefficients and can be solve by an efficient iterative numerical method; we have used SQLM in this work. The SQLM procedure is as follows;

- We transform our domain in η to $[0, J]$, where $J \in \mathbb{Z}^+$ is the far field limit of the boundary.
- Transformation mapping of $\eta = \frac{(\chi + 1)}{2} J$ to the computational domain $[-1, 1]$ where the method is applicable.
- We approximate the unknown functions f_{a+1}, θ_{a+1} and ϕ_{a+1} by Chebyshev interpolating polynomials and the derivatives of the approximating functions at Gauss–Lobatto collocation points.

$$\chi_i = \cos\left(\frac{\pi i}{N}\right), \quad \chi \in [-1, 1], \quad i = 0, 1, 2, 3, 4, \dots, N. \quad (4.7)$$

N is the number of collocation points.

- We used the Chebyshev differentiation matrix D stated as, see Trefthen⁴²

$$\left\{ \begin{array}{l} \frac{d^n f_{a+1}(\chi_i)}{d\chi} = \sum_{k=0}^N D_{ik}^n f_{a+1}(\chi_k) = \mathbf{D}^n \mathbf{F}, \\ \frac{d^n \theta_{a+1}(\chi_i)}{d\chi} = \sum_{k=0}^N D_{ik}^n \theta_{a+1}(\chi_k) = \mathbf{D}^n \mathbf{T}, \\ \frac{d^n \phi_{a+1}(\chi_i)}{d\chi} = \sum_{k=0}^N D_{ik}^n \phi_{a+1}(\chi_k) = \mathbf{D}^n \mathbf{P}, \end{array} \right. \quad (4.8)$$

$$\text{where } \mathbf{D} = \frac{2D}{J}, \quad \mathbf{F} = [f_{a+1}(\chi_0), f_{a+1}(\chi_1), \dots, f_{a+1}(\chi_N)]^T, \quad \mathbf{T} = [\theta_{a+1}(\chi_0), \theta_{a+1}(\chi_1), \dots, \theta_{a+1}(\chi_N)]^T \text{ and } \mathbf{P} = [\phi_{a+1}(\chi_0), \phi_{a+1}(\chi_1), \dots, \phi_{a+1}(\chi_N)]^T.$$

Evaluating Eqs. (4.1)–(4.3) at the collocation points and substituting derivatives of Eq. (4.8) yields a simultaneous systems

$$\mathbf{E}_{11} \mathbf{F}_{a+1} + \mathbf{E}_{12} \mathbf{T}_{a+1} + \mathbf{E}_{13} \mathbf{P}_{a+1} = \mathbf{R}_{b_1} \quad (4.9)$$

$$\mathbf{E}_{21} \mathbf{F}_{a+1} + \mathbf{E}_{22} \mathbf{T}_{a+1} + \mathbf{E}_{23} \mathbf{P}_{a+1} = \mathbf{R}_{b_2} \quad (4.10)$$

$$\mathbf{E}_{31} \mathbf{F}_{a+1} + \mathbf{E}_{32} \mathbf{T}_{a+1} + \mathbf{E}_{33} \mathbf{P}_{a+1} = \mathbf{R}_{b_3} \quad (4.11)$$

where

$$\left\{ \begin{array}{l} E_{11} = \text{diag}[\xi_{1,a}] \mathbf{D}^3 + \text{diag}[\xi_{2,a}] \mathbf{D}^2 + \text{diag}[\xi_{3,a}] \mathbf{D} + \text{diag}[\xi_{4,a}] \mathbf{I}, \\ E_{12} = \text{diag}[\xi_{5,a}] \mathbf{D} + \text{diag}[\xi_{6,a}] \mathbf{I}, \quad E_{13} = \mathbf{0}_{N+1 \times N+1} \\ E_{21} = \text{diag}[\xi_{7,a}] \mathbf{D}^2 + \text{diag}[\xi_{8,a}] \mathbf{D} + \text{diag}[\xi_{9,a}] \mathbf{I}, \\ E_{22} = \text{diag}[\xi_{10,a}] \mathbf{D}^2 + \text{diag}[\xi_{11,a}] \mathbf{D} + \text{diag}[\xi_{12,a}] \mathbf{I}, \\ E_{23} = \text{diag}[\xi_{13,a}] \mathbf{D} \\ E_{31} = \text{diag}[\xi_{14,a}] \mathbf{D} + \text{diag}[\xi_{15,a}] \mathbf{I}, \quad E_{32} = \text{diag}[\xi_{16,a}] \mathbf{D}^2 \\ E_{33} = \text{diag}[\xi_{17,a}] \mathbf{D}^2 + \text{diag}[\xi_{18,a}] \mathbf{D} + \text{diag}[\xi_{19,a}] \mathbf{I} \end{array} \right. \quad (4.12)$$

subject to the spectral boundary conditions

$$\begin{aligned} f_{a+1}(\chi_N) = 1, \quad \sum_{k=0}^N D_{N,k} f_{a+1}(\chi_k) = 1, \quad \theta_{a+1}(\chi_N) = 1, \quad \phi_{a+1}(\chi_N) = 1. \\ f_{a+1}' = \sum_{k=0}^N D_{0,k} f_{a+1}(\chi_k) = 0, \quad \theta_{a+1}(\chi_0) = 0, \quad \phi_{a+1}(\chi_0) = 0. \end{aligned} \quad (4.13)$$

In addition, we have used the following as our initial approximation to kick start our iterative scheme.

$$f_0(\eta) = 1 - e^{-\eta}, \quad \theta_0(\eta) = e^{-\eta}, \quad \phi_0(\eta) = e^{-\eta}.$$

4.1. Numerical validation

Numerous researchers have established the efficiency, accuracy and convergence of the SQLM^{39,40}. In this section, we show the convergence of the method and validate the present research work with the work of Malik et al.⁴³, Alsaedi et al.⁴⁴ and Naseem et al.⁴⁵ to ascertain the accuracy and efficiency of the method. We will like to mention MAPLE 18 was used for simulation on an intel 3 GB RAM PC. Table 1 is for the convergence analysis, we observed a rapid convergence of the Spectral quasi-linearization method (SQLM) after six iterations. Tables 2 and 3 show that the current results compare favourably with the previous established result in some limiting conditions.

5. Results and discussion

This article is devoted to develop a mathematical model for Eyring–Powell nanofluid with varying viscosity and thermal conductivity in the presence of heat source and chemical reaction. In order to clearly ascertain the role of various sundry parameters entering flow formation, heat and mass transfer, we present graphical illustrations to show the

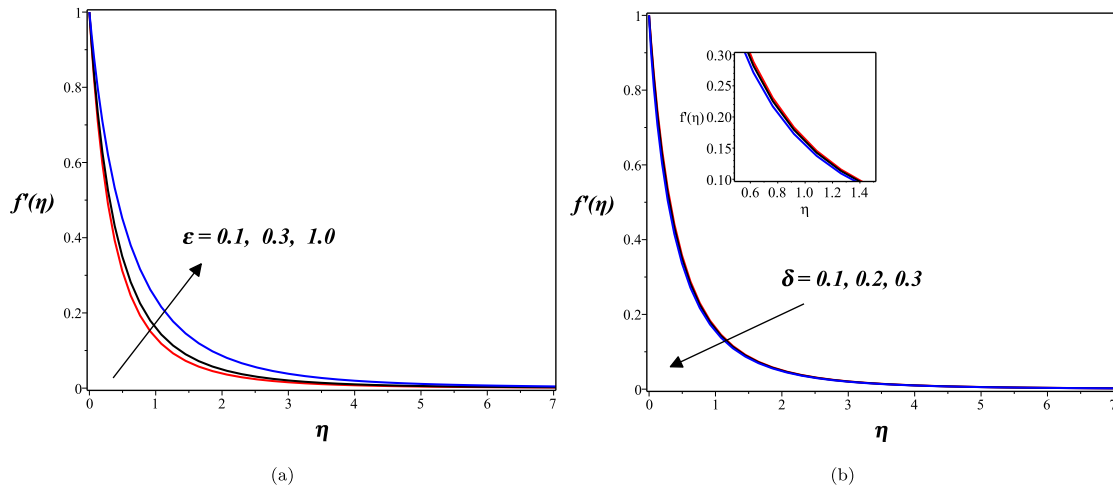


Fig. 2. Influence of fluid parameters (ϵ) and (δ) on the fluid velocity (f') profile.

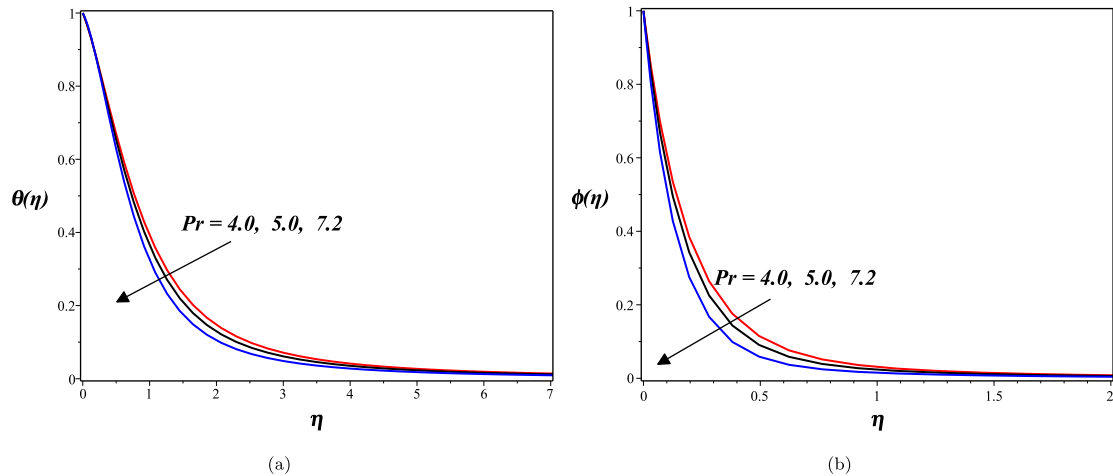


Fig. 3. Influence of Prandtl number (Pr) on the fluid temperature (θ) and concentration (ϕ) profiles.

Table 1

Convergence analysis of the spectral quasi-linearization method (SQLM) for $-f''(0)$, $-\theta'(0)$ and $-\phi'(0)$ for the following parameter values of $\beta_1 = 0.5$, $\beta_2 = 0.5$, $\delta = 0.2$, $\Lambda = 2.5$, $\epsilon = 0.3$, $M = 1.0$, $\lambda_1 = 0.2$, $\lambda_2 = 0.2$, $Ec = 0.4$, $R = 0.4$, $P_r = 7.2$, $L_e = 0.03$, $\theta_w = 1.8$, $Nb = 1.0$, $Nt = 0.5$, $K_r = 1.2$.

Iterations	Spectral quasi-linearization method (SQLM)			CPU(s)
	$-f''(0)$	$-\theta'(0)$	$-\phi'(0)$	
n				Time
2.0	2.7274557158	0.8413093451	0.7315857223	2.609
4.0	2.7613146123	0.8400529799	0.7321360655	4.156
6.0	2.7613146135	0.8400529799	0.7321360656	6.094
8.0	2.7613146135	0.8400529799	0.7321360656	8.187
10.0	2.7613146135	0.8400529799	0.7321360656	10.245

Table 2

Comparison of Skin friction coefficients ($-f''(0)$) for different values of M when $\beta_1 = \epsilon = \Lambda = 0$ and $\delta = 0$.

Values	Malik et al. ⁴³	Alsaedi et al. ⁴⁴	Naseem et al. ⁴⁵	Present result
M	$-f''(0)$	$-f''(0)$	$-f''(0)$	$-f''(0)$
0.0	1.00000	1.00000	1.00000	1.00000
0.5	1.11802	1.11803	1.11802	1.11803
1.0	-1.41419	1.41421	1.41420	1.41421

effects of some physical parameters with detail explanation as to their importance on the velocity, temperature and concentration profiles. Keeping this in mind, we assume the following initial value for each

Table 3

Comparison of Skin friction coefficients ($-f''(0)$) for different values of Λ when $\beta_1 = \epsilon = M = 0$ and $\delta = 0$.

Values	Sharidan et al. ⁴⁶	Chamkha et al. ⁴⁷	Kumar & Srinivas ⁴⁸	Present result
Λ	$-f''(0)$	$-f''(0)$	$-f''(0)$	$-f''(0)$
0.8	1.261042	1.261512	1.26108	1.261042
1.2	1.377722	1.378052	1.37777	1.377723

parameter.

$$\begin{cases} \beta_1 = 0.5, \beta_2 = 0.5, \delta = 0.2, \Lambda = 2.5, \epsilon = 0.3, M = 1.0 \\ \lambda_1 = 0.2, \lambda_2 = 0.2, Ec = 0.4, R = 0.4, P_r = 7.2. \\ L_e = 1.5, \theta_w = 1.8, Nb = 1.0, Nt = 0.5, K_r = 1.2. \end{cases} \quad (5.1)$$

unless stated otherwise.

The fluid parameters ϵ and δ have an opposing effect on the flow velocity as depicted in Fig. 2. An increment in ϵ shows a sharp decrease in the viscosity of the fluid which thus led to enhancement of the fluid velocity. In contrast δ shows underwhelming effect on the velocity of the fluid. Fig. 3 shows the influence of Prandtl number on the temperature and concentration profiles. We observed that the Eyring–Powell fluid conduct and diffuse lesser as we increase the Prandtl number. This is due to reduction in the thermal boundary layer, which has a great impact on the shear stress. This implies heat loss is experienced to immediate working environment which consequently led to a reduction

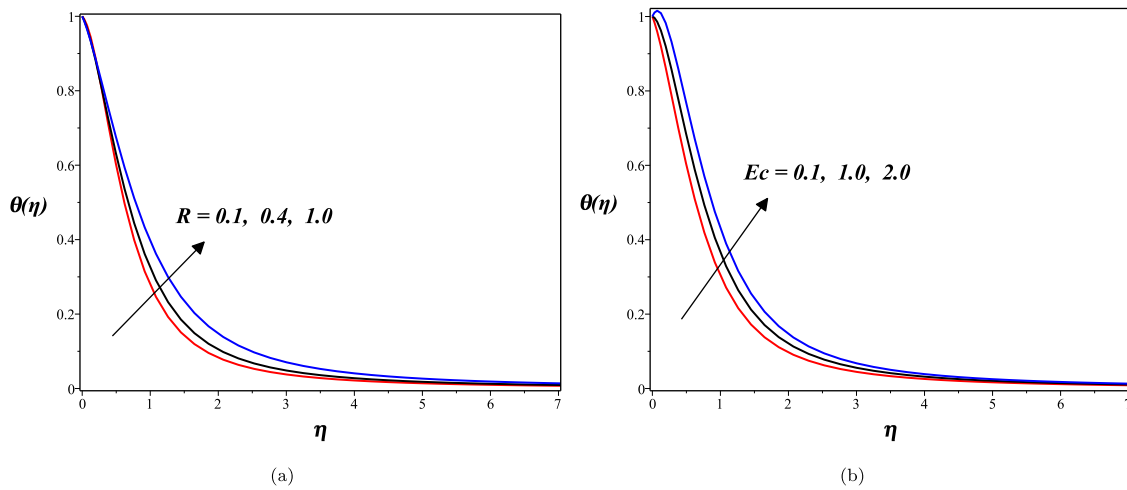


Fig. 4. Influence of Radiation (R) and Eckert numbers (Ec) on the fluid temperature (θ) profile.

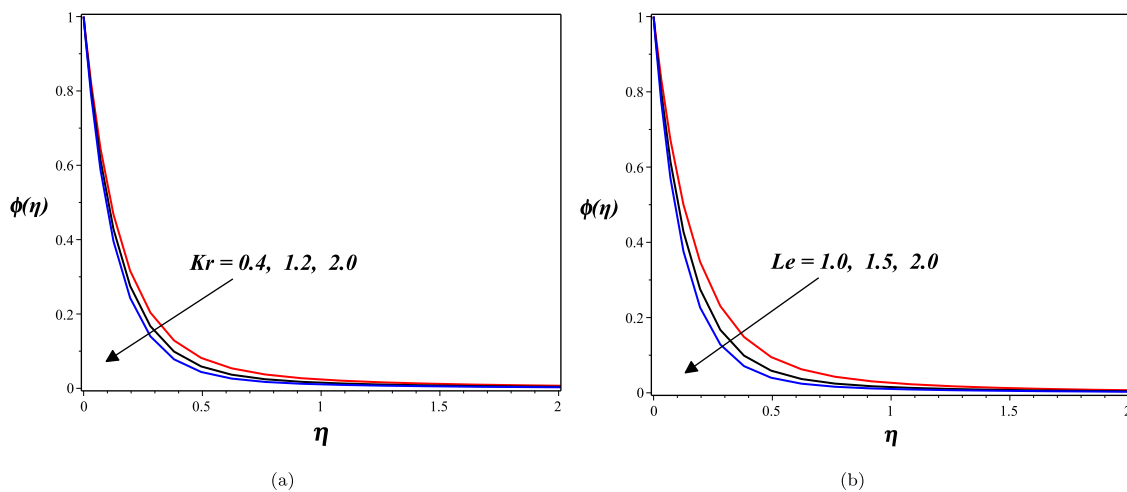


Fig. 5. Influence of chemical reaction (Kr) and Lewis numbers (Le) on the fluid concentration (ϕ) profile.

in the energy profile. Interestingly, this observation agrees with the report of Malik et al.⁴³ A similar explanation suffices as to the reduction in the concentration profile as we increase the Prandtl number as shown in Fig. 3(b). The influence of Radiation parameter R on the energy profile is well pronounced; see Fig. 4(a). The Eyring–Powell fluid conducts and conserves much energy as we increase the radiation number. A similar observation was reported in the study conducted by Hayat et al.²⁵

In similar manner like the radiation parameter, increment in Eckert number Ec leads to increment in the temperature field. This can be attributed to the fact that as Eckert number increases, heat is produced as a result of the drag between the fluid particles, thus, heat production inside the fluid rises with additional heating due to viscous dissipation, as in Fig. 4(b). Chemical reaction parameter K_r and Lewis number L_e have similar effect on the concentration profile. Fig. 5 shows that enhancement of K_r and L_e retard the concentration profile. In case of the Lewis number $L_e = \frac{\alpha}{D_B}$, we note here that L_e is inversely proportional to Brownian motion coefficient D_B thus reduction in the fluid particle interaction which lead to reduction in the concentration profile as depicted in Fig. 5(b).

One of the novelties of this work is to examine the influence of Brownian motion parameter Nb and thermophoresis Nt effects. In Figs. 6 and 7, these two effects are clearly illustrated graphically. We observed that increasing the Brownian motion parameter increases the

temperature profile but an adverse effect was noticed on the concentration profile. For the thermophoresis parameter both the temperature and concentration profiles are significantly influenced. We understand these results as increasing thermophoresis parameter lead to more collision of the fluid particles thus, high energy is produced which in turn increase the reaction taking place in the system. This accounted for the temperature and concentration increase.

Fig. 8(a) and (b), shed more light on the behaviour of space and heat generation parameter λ_1 and λ_2 on the temperature profile, as expected increase in heat and space generation parameter lead to increase in the temperature profile. Fig. 8(c) shows an escalating effect on the temperature profile as the temperature ratio θ_w increases. The behaviour of the three parameters in Fig. 8 are quite not surprising because they are temperature associated parameters. In Fig. 9, it was observed that an inverse relation exists between the Lorentz force and the velocity profiles. Physically, the magnetic field intensity is a retarding force in the flow profile. Conversely, displaying an increase in the thermal boundary layer.

Fig. 10(a) depicts the impact of variable viscosity parameter on fluid velocity. It is interesting to observe that the variable viscosity parameter act as a decreasing function on fluid velocity. This could be clearly attributed to the fact that increase in β_1 implies increase in fluid viscosity, which in turn increases the shear stress and thereby retarding flow formation. Fig. 10(b) exhibits an increase in the Eyring–Powell

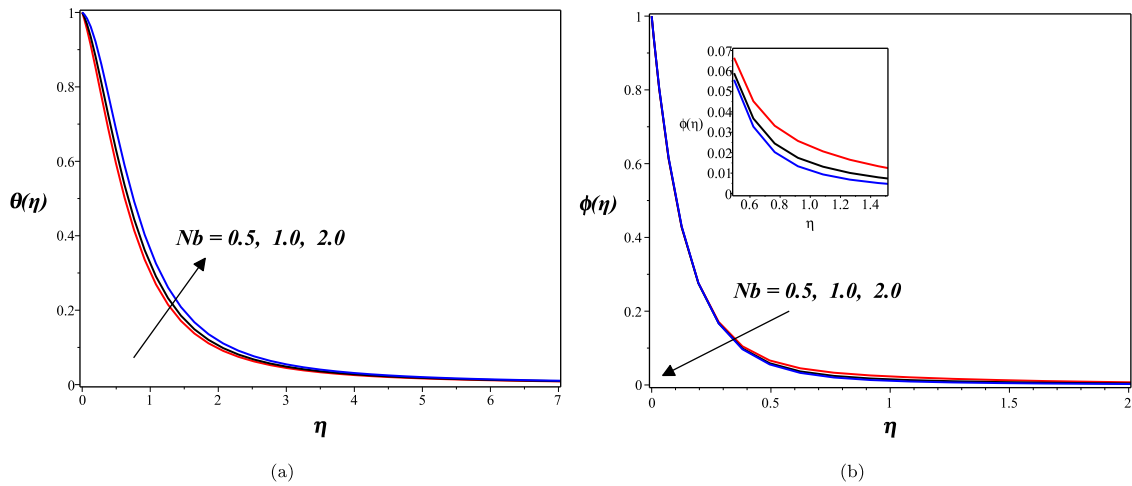


Fig. 6. Influence of Brownian motion parameter (N_b) on the fluid temperature (θ) and concentration (ϕ) profiles.

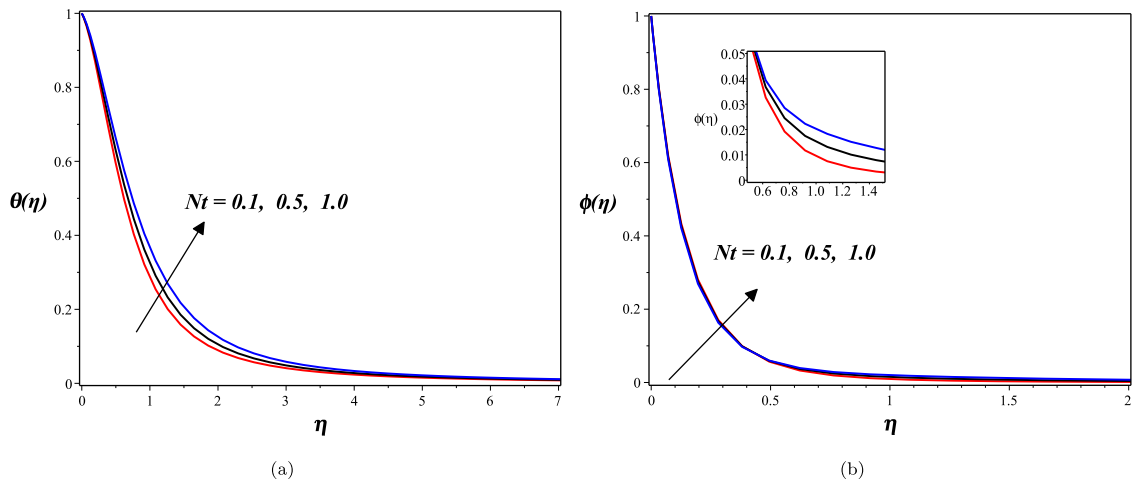


Fig. 7. Influence of thermophoresis parameter (N_t) on the fluid temperature (θ) and concentration (ϕ) profiles.

fluid’s temperature profile as the temperature dependent thermal conductivity parameter β_2 increases, which in turn affects the boundary layer’s ability to create heat and assisting temperature profiles.

Table 4 shows the effect of varying sundry parameters on the skin friction, Nusselt and Sherwood number coefficients. For the parameter under consideration, the values of the skin friction coefficient are all negative. We observe the skin drag force increases as the variable dynamical viscosity and variable thermal conductivity parameter increases, whereas the Nusselt number decreases as we increases the variable dynamical viscosity. Enhancing the fluid parameter ϵ and magnetic parameter abates the skin friction and Nusselt number but augments the Sherwood number coefficient. The effects of radiation and Lewis number on $Re_x^{\frac{1}{2}} C_f$, $Re_x^{\frac{1}{2}} Nu$ and $Re_x^{\frac{1}{2}} Sh$ are diametrically opposed. The behaviour of fluid parameter δ , Brownian parameter N_b and chemical reaction parameter K_r , on the engineering physical quantities are similar. Increasing the thermophoresis parameter enhances skin drag forces but diminishes Nusselt and Sherwood number.

6. Conclusion

The influence of certain thermo-physical characteristics on the flow of Eyring–Powell fluid across a stretched sheet was investigated in this work. We presented the governing equations in ordinary differential after employing a suitable similarity transformation. An efficient iterative scheme SQLM was employed to give account of all the flow

parameters after numerical validation with earlier known works have been established. The findings can be summarized as follows:

- Enhancement of temperature dependent viscosity parameter lead to reduction in the fluid flow profile. However, enhancement of temperature dependent thermal conductivity increases the energy profile
- Increasing the Brownian motion parameter increases the thermal boundary layer but opposed the specie boundary layer.
- Thermophoresis parameter has a direct proportionality with the build-up of thermal and specie boundary layers.
- Radiation has an escalating effect on the temperature profile.
- Chemical reaction and Lewis numbers retard the concentration profile.
- Prandtl number has a pronounced effect on the temperature and concentration profiles.

To this end, we recommend increasing the Brownian motion, radiation and thermophoresis coefficients as a means to increase the conductivity of the Eyring–Powell nanofluid taking into account heat source and magnetic field intensity in both momentum and energy equations. The SQLM prove its uniqueness, worth, simplicity, stability and ability in this study. Thus, the method can be employ to provide approximate solution to different fluid rheology problem in any flow geometry.

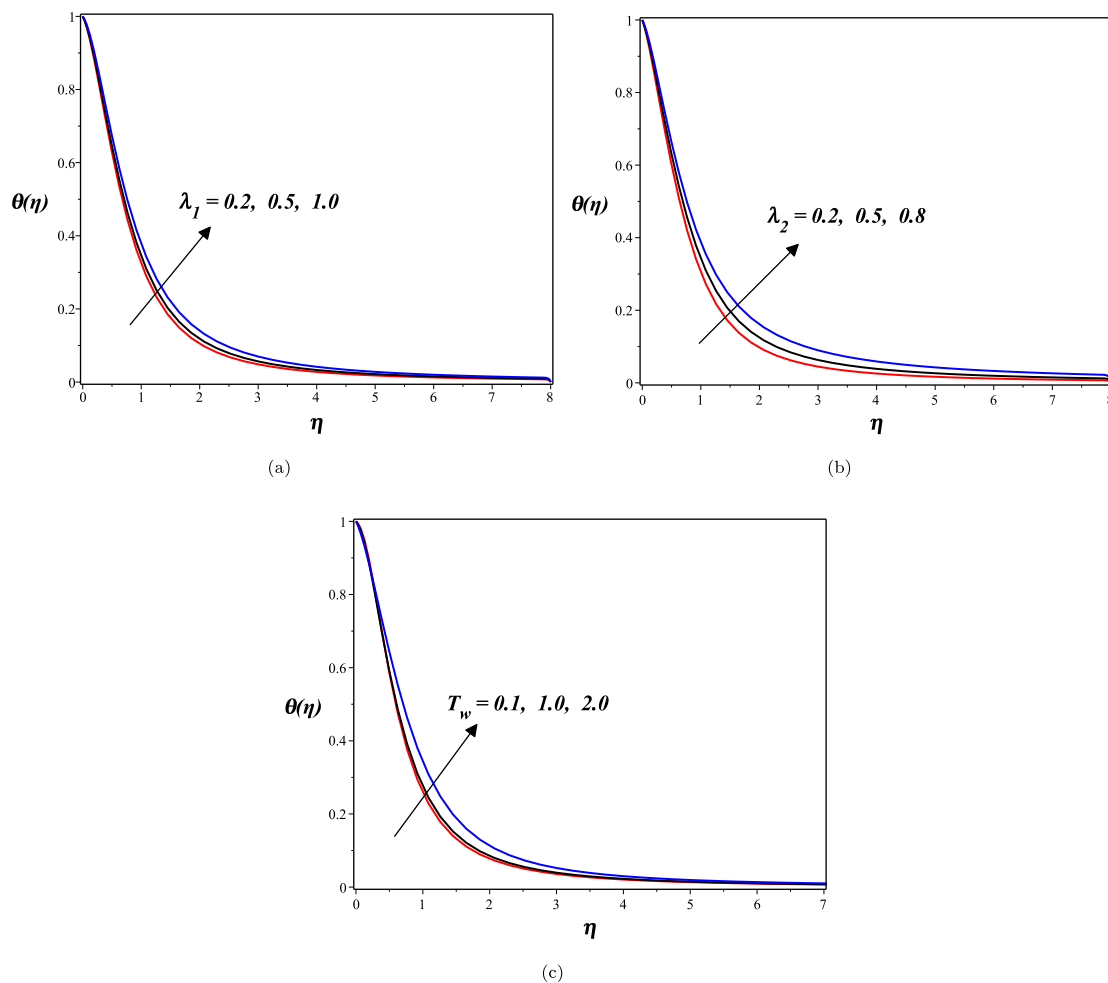


Fig. 8. Influence of space generation (λ_1), heat generation (λ_2) and temperature ratio parameters (θ_w) on the fluid temperature (θ) profile.

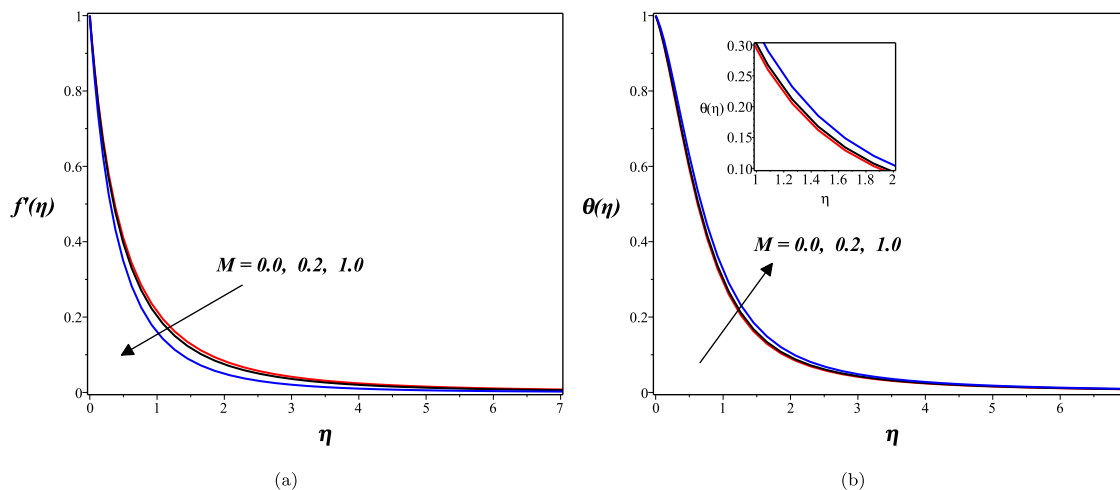


Fig. 9. Influence of Magnetic parameter (M) on the velocity f' and temperature (θ) profiles.

Declaration of competing interest

The authors declare that they have no known competing financial interests or personal relationships that could have appeared to influence the work reported in this paper.

Acknowledgements

The authors are grateful to the two reviewers for their thoughtful comments, which have significantly enhanced the manuscript presentation.

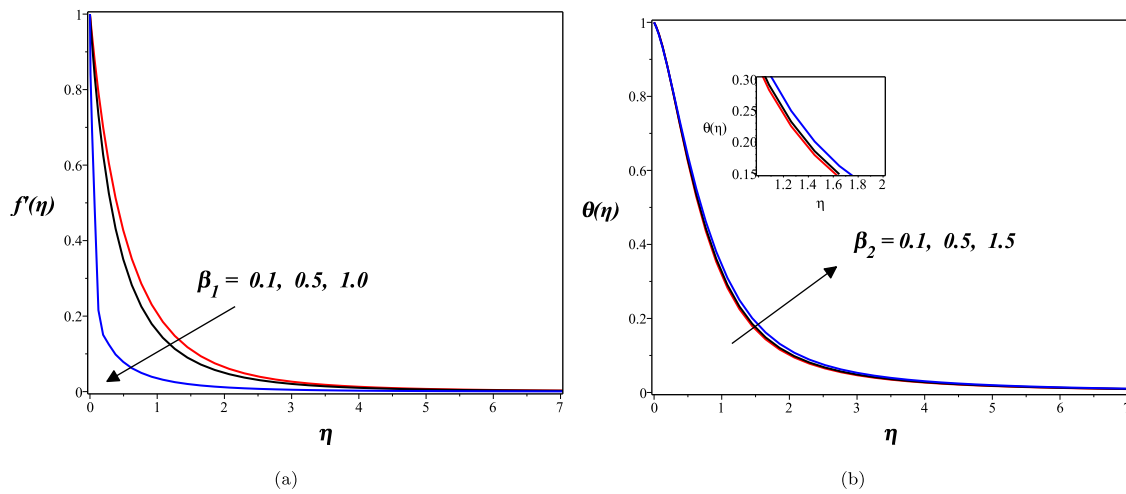


Fig. 10. Influence of variable viscosity parameter (β_1) and variable thermal conductivity on the velocity f' and temperature (θ) profiles.

Table 4

Numerical values of skin friction coefficient $Re_x^{-\frac{1}{2}} C_f$, heat transfer coefficient $Re_x^{-\frac{1}{2}} Nu$ and mass transfer coefficient $Re_x^{-\frac{1}{2}} Sh$ for different values of $\beta_1, \beta_2, \delta, \epsilon, M, R, L_e, Nb, Nt, K_r$, when $P_r = 7.2, \lambda_1 = 0.2, \lambda_2 = 0.2, A = 2.5, Ec = 0.5, \theta_w = 1.2$.

β_1	β_2	δ	ϵ	M	R	L_e	Nb	Nt	K_r	$Re_x^{-\frac{1}{2}} C_f$	$Re_x^{-\frac{1}{2}} Nu$	$Re_x^{-\frac{1}{2}} Sh$
0.1	0.5	0.2	0.3	1.0	0.2	0.03	1.0	0.5	1.2	-2.152135	1.601805	0.822626
0.2										-2.074689	1.598495	0.821990
0.5										-1.794622	1.578650	0.821028
0.5	0.1									-1.796702	1.246393	0.827680
	0.2									-1.796172	1.330737	0.825467
	0.5									-1.794622	1.578650	0.821028
		0.1								-1.837438	1.603566	0.815813
		0.2								-1.794622	1.578650	0.821028
		0.3								-0.781085	1.561767	0.822975
			0.1							-1.602736	1.663672	0.796327
			0.3							-1.794622	1.578650	0.821028
			0.4							-1.889825	1.547160	0.830407
				0.1						-1.592073	2.193129	0.684892
				0.2						-1.636599	2.066184	0.712571
				1.0						-1.794622	1.578650	0.821028
					0.1					-1.795308	1.374811	0.828101
					0.2					-1.794622	1.578650	0.821028
					0.5					-1.792352	2.170670	0.809218
						0.01				-1.808358	2.091168	0.162108
						0.02				-1.800627	1.800285	0.505591
						0.03				-1.795866	1.624377	0.751100
							0.5			-1.807888	2.039732	0.482589
							1.0			-1.794622	1.578650	0.821028
							2.0			-1.774282	0.997642	0.948793
								0.1		-1.817323	2.371676	0.832235
								0.5		-1.807888	2.039732	0.482589
								1.0		-1.798055	1.727764	0.275820
									0.4	-1.800528	1.814181	0.011724
									1.2	-1.798055	1.727764	0.275820
									1.5	-1.797276	1.700593	0.362134

References

- Choi S. Enhancing thermal conductivity of fluids with nanoparticles. *JASME-Publ Fed.* 1995;31:99-106.
- Masuda H, Ebata A, Teramae K, Hishinuma N. Alteration of thermal conductivity and viscosity of liquid by dispersing ultra-fine particles. *Netsu Bussei.* 1999;31:227-233.
- Buongiorno J. Convective transport in nanofluids. *ASME J Heat Transf.* 2006;128:240-250.
- Khanafer K, Vafai M. Buoyancy-driven heat transfer enhancement in a two-dimensional enclosure utilizing nanofluids. *Int J Heat Mass Transfer.* 2003;46:3639-3653.
- Abu-Nada E. Application of nanofluids for heat transfer enhancement of separated flows encountered in a backward facing step. *Int J Heat Fluid Flow.* 2008;29:242-249.
- Neild DA, Kuznetsov AV. The cheng-minkowycz problem for natural convective boundary layer flow in a porous medium saturated by a nanofluid. *Int J Heat Mass Transfer.* 2009;52:5792-5795.
- Grosan T, Pop I. Fully developed mixed convection in a vertical channel filled by a nanofluid. *ASME J Heat Transf.* 2012;134:82501-82505.
- Sakiadis BC. Boundary-layer behaviour on continuous solid surfaces: I, boundary layer equations for two-dimensional and axisymmetric flow. *Am Inst Chem Eng J.* 1961;7:26-28.
- Crane LJ. Flow past a stretching plate. *Z Angew Math Phys.* 1970;21:645-647.
- Magyari E, Keller B. Exact solutions for self-similar boundary-layer flows induced by permeable stretching walls. *Euro J Mech B/Fluids.* 2000;19:109-122.
- Ishak A, Nazar I, Pop R. Boundary layer flow and heat transfer over an unsteady stretching vertical surface. *Meccanica.* 2009;44:369-375.
- Wang CY. Liquid film on an unsteady stretching sheet. *Q Appl Math.* 1990;48:601-610.
- Kasali KB, Tijani YO, Lawal MO, Lawal YT. Soret dufour and radiation effects of a viscoelastic fluid on an exponentially stretching surface using the catteneo-christov heat flux model. *Multidiscip Model Mater Struct.* 2020;16(6):1577-1594.
- Powell R, Eyring HL. Mechanisms for the relaxation theory of viscosity. *Nature.* 1944;154(4):427-428.
- Javed T, Ali N, Abbas Z, Sajid M. Flow of an eyring-Powell non-Newtonian fluid over a stretching sheet. *Chem Eng Commun.* 2013;200(3):327-336.

16. Hayat T, Iqbal Z, Qasim M, Obaidat S. Steady flow of an eyring-Powell fluid over a moving surface with convective boundary conditions. *Int J Heat Mass Transf.* 2012;55(7):1817–1822.
17. Ogunseye HA, Sibanda P, Mondal H. Mixed convective stagnation-point flow of eyring-Powell nanofluid over stretching cylinder with thermal slip conditions. *J Cent South Univ.* 2019;26:1172–1183.
18. Ogunseye HA, Tijani YO, Sibanda P. Entropy generation in an unsteady eyring-Powell hybrid nanofluid flow over a permeable surface: A Lie group analysis. *Heat Transfer.* 2020:1–17.
19. Ogunseye HA, Salawu SO, Tijani M, Sibanda P. Dynamical analysis of hydromagnetic Brownian and thermophoresis effects of squeezing eyring–Powell nanofluid flow with variable thermal conductivity and chemical reaction. *Multidiscip Model Mater Struct.* 2019;01(08):1573–6105.
20. Akbar NS, Ebaid A, Khan ZH. Numerical analysis of magnetic field effects on eyring-Powell fluid flow towards a stretching sheet. *J Magn Magn Mater.* 2015;282:355–358.
21. Agbaje TM, Mondal S, Motsa SS, Sibanda P. A numerical study of unsteady non-Newtonian Powell-eyring nanofluid flow over a shrinking sheet with heat generation and thermal radiation. *Alex Eng J.* 2017;56(1):81–91.
22. Ibrahim W, Gadisa G. Finite element method solution of boundary layer flow of Powell-eyring nanofluid over a non-linear stretching surface. *J Appl Math.* 2019. <http://dx.doi.org/10.1155/2019/3472518>.
23. Babu JM, Seep N, Raju CSK. Heat and mass transfer in MHD eyring-Powell nanofluid flow due to cone in porous medium. *Int J Eng Res Afr.* 2015;19:57–74.
24. Jalil M, Asghar S, Imran SM. Self-similar solutions for the flow and heat transfer of Powell-eyring fluid over a moving surface in a parallel free stream. *Int J Heat Mass Transfer.* 2013;65:73–79.
25. Hayat T, Asad S, Mustafa M, Alsaedi A. Radiation effects on the flow of Powell-eyring fluid past an unsteady inclined stretching sheet with non-uniform heat source/sink. *PLoS One.* 2014;9(7):e103214.
26. Ramzan M, Bilal M, Kanwal S, Chung JD. Effects of variable thermal conductivity non-linear thermal radiation past an eyring-Powell nanofluid flow with chemical reaction. *Commun Theor Phys.* 2017;67(6):723–731.
27. Malik MY, Khan I, Hussain A, Salahuddin T. Mixed convection flow of MHD eyring-Powell nanofluid over a stretching sheet: A numerical study. *AIP Adv.* 2015;5(11):117–118.
28. Inman RM. Experimental study of temperature distribution in laminar tube flow of a fluid with internal heat generation. *Int J Heat Mass Transfer.* 1962;5:1053–1063.
29. Ostrach S. Laminar natural convection flow and heat transfer of fluids with and without heat sources in channels with constant wall temperatures. *NACA TN.* 1952.
30. Toor HL. Heat transfer in forced convection with internal heat generation. *J Am Inst Chem Eng.* 1958;4:319–323.
31. Chambre PL. Laminar boundary layer with distributed heat sources or sinks. *Appl Sci Res A.* 1957;6:393–401.
32. Foraboschi FP, Federico ID. Heat transfer in laminar flow of non-Newtonian heat generating fluids. *Int J Heat Mass Transfer.* 1964;7:315–318.
33. Jha BK, Ajibade AO. Unsteady free convection couette flow of heat generating/absorbing fluids between vertical porous plates with periodic heat input. *Int Communi Heat Mass Transfer.* 2009;36:624–631.
34. Adesanya SO. Free convective flow of heat generating fluid through a porous vertical channel with velocity slip and temperature jump. *Ain Shams Eng J.* 2015;6:1045–1052.
35. Jha BK, Oni MO, Aina B. Steady fully developed mixed convection flow in a vertical micro-concentric-annulus with heat generating/absorbing fluid: an exact solution. *Ain Shams Eng J.* 2016;9(4):1289–1301.
36. Oni MO. Combined effect of heat source, porosity and thermal radiation on mixed convection flow in a vertical annulus: An exact solution. *Eng Sci Tech Int J.* 2017;20(2):518–527.
37. Mkhatshwa MP, Motsa SS, Sibanda P. MHD mixed convective radiative flow of eyring-Powell fluid over an oscillatory stretching sheet using bivariate spectral method on overlapping grids. *Heat Transfer.* 2020:1–33.
38. Bellman RE, Kalaba RE. *Quasi Linearization and Nonlinear Boundary-Value Problems.* New York: Elsevier; 1965.
39. Motsa SS. A new spectral local linearization method for nonlinear boundary layer flow problems. *J Appl Math.* 2013;013:423628.
40. Motsa SS, Sibanda P. On extending the quasilinearization method to higher order convergent hybrid schemes using the spectral homotopy analysis method. *J Appl Math.* 2013;879195.
41. Akolade MT, Tijani YO. A comparative study of three dimensional flow of Casson–Williamson nanofluids past a riga plate: Spectra quasi-linearization approach. *Part Differ Equ Appl Math.* 2021;4:100108.
42. Trefethen LN. *Spectral Methods in MATLAB.* SIAM; 2000:10.
43. Malik MY, Khan I, Hussain A, Salahuddin T. Mixed convection flow of MHD eyring-Powell nanofluid over a stretching sheet: A numerical study. *AIP Adv.* 2015;5(11):117–118.
44. Alsaedi A, Khan MI, Farooq M, Gull N, Hayat T. Magnetohydrodynamic (MHD) stratified bioconvective flow of nanofluid due to gyrotactic microorganisms. *Adv Powder Technol.* 2017;28(1):288–298.
45. Naseem F, Shafiq A, Zhao Lifeng, Naseem A. MHD biconvective flow of Powell eyring nanofluid over stretched surface. *AIP Adv.* 2017;7:065013.
46. Sharidan S, Mahmood T, Pop I. Similarity solutions for the unsteady boundary layer flow and heat transfer due to a stretching sheet. *Int J Appl Mech Eng.* 2006;11:647–654.
47. Chamkha AJ, Aly AM, Mansour MA. Similarity solution for unsteady heat and mass transfer from a stretching surface embedded in a porous medium with suction/injection and chemical reaction effects. *Chem Eng Commun.* 2010;197(6):846–858.
48. Kumar B, Srinivas S. Unsteady hydromagnetic flow of eyring-Powell nanofluid over an inclined permeable stretching sheet with joule heating and thermal radiation. *J Appl Comput Mech.* 2020;6(2):259–270.